

A Three Dimensional Numerical Investigation of the T_{ϵ}^* integral along a Curved Crack Front

J. H. Jackson¹, A. S. Kobayashi², S. N. Atluri³

Abstract: The T_{ϵ}^* integral was calculated numerically along an extending, tunneling crack front in an 8 mm thick, aluminum three-point bend (3PB) specimen, using a numerical model driven by experimentally obtained surface displacements. The model provided input to a contour integration for the T_{ϵ}^* integral, via the Equivalent Domain Integral (EDI) method with incremental plasticity. Validity of the analysis was ensured by the agreement of the T_{ϵ}^* integral obtained on the surface (plane stress) and the plane stress values from previous studies. T_{ϵ}^* was observed to decrease from the outer surface of the specimen to the more constrained mid-plane. This difference became more pronounced as the crack grew.

keyword: T_{ϵ}^* integral, 3-D fracture, CTOA, stable crack growth, crack tunneling.

1 Introduction

A majority of practical fracture mechanics problems involve complex, three-dimensional (3-D) geometries. Although a two-dimensional (2-D) analysis will often yield acceptable results, a complete analysis requires a full, 3-D approach. In light of this, analysis of fracture parameters along crack fronts of three-dimensional flaws has been considered for several years now. The most recent studies have involved those of the elastic-plastic J -integral [Rice (1968)] whose 3-D calculation is not a trivial task. Several authors have overcome much of the difficulty associated with 3-D J calculation. Most notably, methods of Virtual Crack Extension (VCE) [Parks, 1977] have been employed by authors such as Shih, Moran, and Nakamura (1986) and Nakamura, Shih, and Freund (1986) to calculate point-wise values of J -integral along a curved crack front.

In similar fashion, the T_{ϵ}^* integral, [Atluri, Nishioka, and Nakagaki (1984)] which is relatively new in comparison, has been studied extensively only in two-dimensional form until recently. As with the J -integral, the natural progression of the study of this parameter has led to the necessity for a three-dimensional analysis. Since the utility of the T_{ϵ}^* integral lies in its assumed ability to characterize stable crack extension, it is desired to extend its 2-D form to a more complete 3-D form. This has implications on the formation of a tunneled crack front in a thick material.

2 Contour Integrals

2.1 3-D J -integral

There are essentially three methods that have been utilized in calculating three-dimensional energy release rate in a numerical analysis. Two involve the VCE method, both direct and indirect as utilized by authors such as Li, Shih and Needleman (1985). The third involves the generalization of the two-dimensional contour integral to a three dimensional surface integral, details of which can be found in papers such as those of Amestoy, Bui, and Labbens (1981) or Raynund and Palusamy (1981). Only the first two offer the ability for quantification of point-wise values along a curved crack front.

Nikishkov and Atluri (1987) utilize a variation of the VCE method to calculate J -integral using an Equivalent Domain Integral (EDI) method. Here, the process of virtual crack extension is approximated through the use of an arbitrary function that is assigned a value of 1 on a near-field contour, and 0 on a far-field contour. After a transformation of relevant quantities to a crack front coordinate system, this allows a straightforward computation of the near-tip J -integral.

It is well known that the J -integral is based on an assumption of non-linear elasticity, and therefore loses its validity under instances of unloading. On the other hand,

¹ 5353 Memorial Drive 1037, Houston, TX, 77007

² University of Washington, Department of Mechanical Engineering, Seattle, WA 98195-2600

³ University of California, Irvine, Aerospace Engineering, 5252 California Ave. Ste 140, Irvine, CA 92612

the T_{ϵ}^* integral has shown promise in 2-D cases as a stable tearing characterization parameter (see e.g. [Brust, Nishioka, Atluri, Nakagaki (1985)], [Okada, Atluri, Omori, and Kobayashi (1999)], and [Brust, McGowan, and Atluri (1986)]). It is therefore natural to expect similar capability in a 3-D case. The purpose of this paper is to detail the use of Nikishkov and Atluri's (1987) J -integral EDI formulation for calculation of the T_{ϵ}^* integral in a 3-D case.

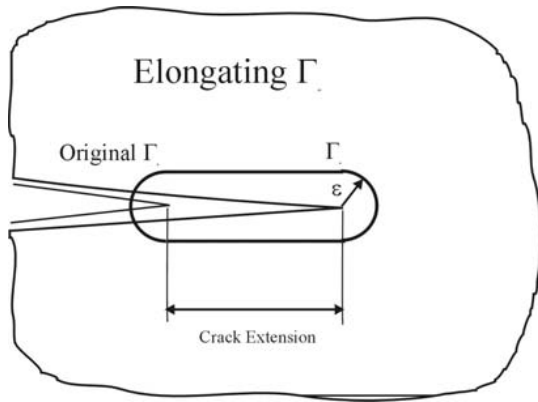


Figure 1 : Elongating Γ_{ϵ} contour for calculation of T_{ϵ}^*

2.2 T_{ϵ}^* integral

The T_{ϵ}^* integral [Stonesifer and Atluri (1982); Atluri, Nishioka, and Nakagaki (1984)], which is essentially an incremental form of the J -integral is seen as a viable means of characterizing stable crack extension. It is calculated along a contour that extends with the moving crack tip (Figure 1) and by virtue of its incremental form, takes into account the entire loading history. A local value of T_{ϵ}^* , defined on a small contour, Γ_{ϵ} closely surrounding the crack tip was given by Brust, Nishioka, Atluri, and Nakagaki (1985) in Eq. 1.

$$T_{1\epsilon}^* = \int_{\Gamma_{\epsilon}} \left(W n_1 - t_i \frac{\partial u_i}{\partial x_1} \right) d\Gamma \quad (1)$$

where t_i are the tractions, u_i are the displacements, n_1 is a unit normal to the crack plane, and W is the strain energy density. The numeral 1 in the subscript is indicative of the fact that the T_{ϵ}^* integral, like the J -integral, is a vector quantity. Here we are concerned only with the x_1 component, which is normal to the crack front. The size of Γ_{ϵ} is typically set at half the specimen thickness to

ensure a state of plane stress along the contour [Okada, Atluri, Omori and Kobayashi (1999)].

A paper by Nikishkov and Atluri (1987) provides the basis for calculation of the T_{ϵ}^* integral via the EDI method. Here it is seen that the EDI method is naturally compatible with isoparametric formulation of finite element (FE) analyses, thus leading to a straightforward numerical integration after extraction of relevant quantities from FEA output.

3 Numerical Model

An 8 mm thick, 3 Point Bend (3PB) specimen (Figure 2) was modeled in the commercial Finite Element Analysis (FEA) code, ABAQUS using 8 node, isoparametric, brick elements (Figure 3). Symmetry allows one quarter of the specimen to be modeled, and the model is further truncated at a specific distance from the crack plane for computational efficiency. This distance was determined by building an initial full quarter model with a relatively coarse mesh of 0.5 mm elements in the vicinity of the crack tip and transitioning to 1.0, and 2.0 mm elements further away. The coarse model contained 4 elements through the half thickness of the specimen.

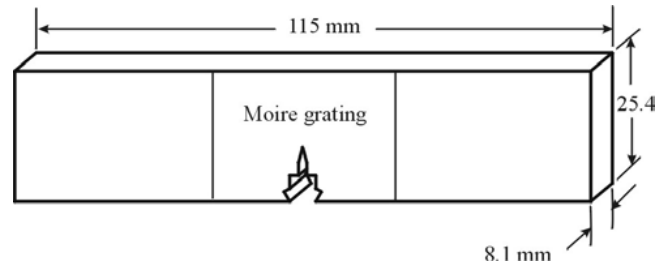


Figure 2 : Three-point bend specimen with moir grating

The coarse model was ramp loaded to a level equivalent with the load at which crack extension was expected to initiate. From experimental observations, this value was taken to be approximately 3.5 kN. The Von Mises stress was then obtained at the centroid of each of the elements through the thickness, at several different distances from the crack face. A truncation distance for prescribing experimentally obtained displacements in the FEA model was determined as the distance from the crack face where Von Mises stress was approximately constant through the thickness. Figure 4 is a typical plot of Von Mises

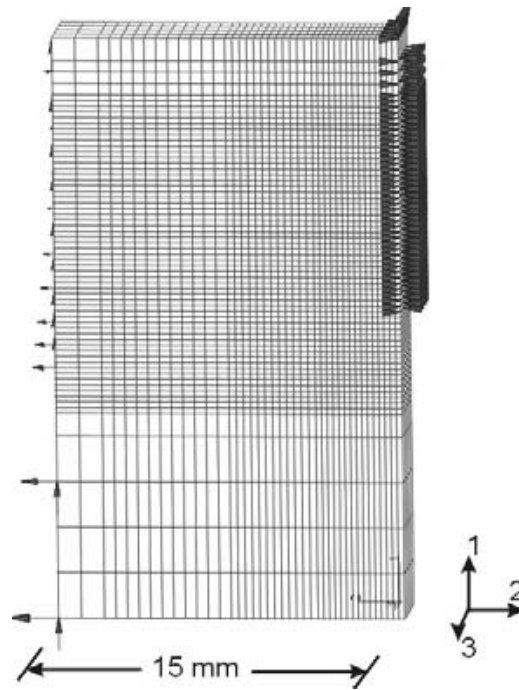


Figure 3 : FEA model truncated at $y=15$ mm, full height

stress through the thickness at a specified distance from the crack plane, and at several points in the x -direction (height). For this analysis, the truncation distance was determined to be at $y = 15$ mm. Figure 5 shows the relatively constant Von Mises stress through the half specimen thickness at a distance of $y=15.0$ mm from the crack plane in comparison to the stress levels shown in figure 4 at a distance of $y = 9.5$ mm from the plane of the crack.

To ensure that the load was applied correctly at the truncation point, and to check possible interaction between the relatively close boundary and the process zone surrounding the crack tip, three different boundary condition application scenarios were explored. Using a simple 2-D FE model, the transverse shear stress was computed along a line 1.0 mm from the truncated boundary. Figure 6 shows three different displacement boundary conditions, which were obtained experimentally using moiré interferometry. The three different forms are: (a) pinned in the middle with linearly varying y -displacement (bending moment) and a single x -displacement applied at the bottom of the specimen, (b) no pin at the mid-span but with linearly varying y -displacement (bending moment) applied, and (c) mid-span pinned and linearly varying y -displacement (bending moment) applied with single x -displacement near the

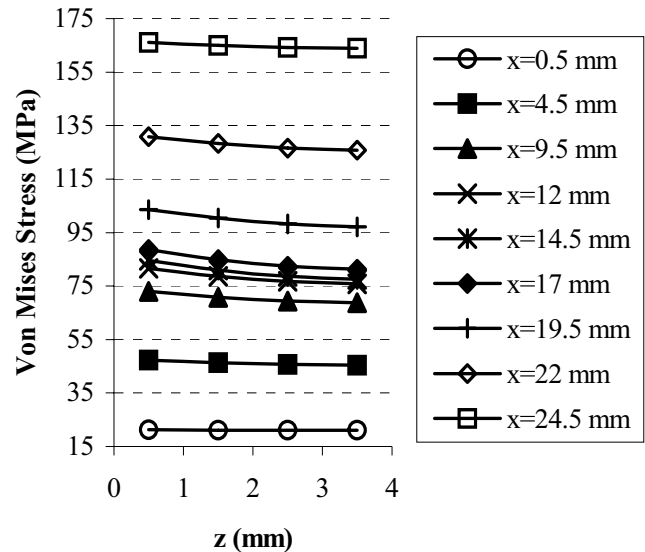


Figure 4 : Von Mises equivalent stress through thickness at $y = 9.5$ mm for $\Delta a = 1.0$ mm and $P=3.5$ KN.

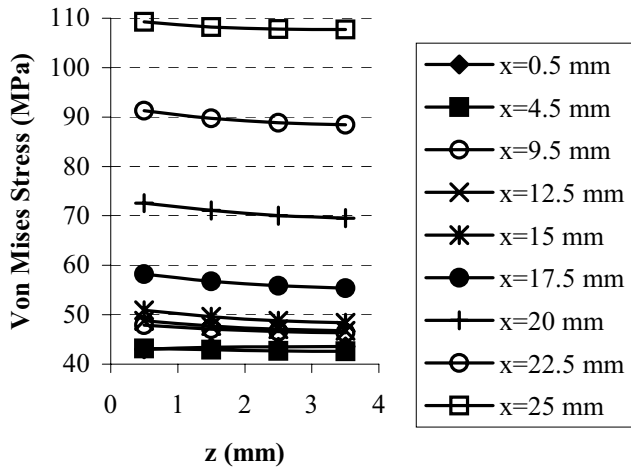


Figure 5 : Von Mises equivalent stress through thickness at $y=15$ mm for $\Delta a = 1.0$ mm and $P=3.5$ KN

middle of the specimen.

No significant interaction effects were noted but only one of the three boundary condition applications resulted in a shear state similar to that obtained in a full, 2-D quarter model. Figure 7 shows the comparison between shear stress distribution 1.0 mm behind the boundary for these three applied transverse displacements and the shear stress distribution seen in an un-truncated model. As shown in Figure 7, the application of boundary conditions in scenario (c) resulted in the best comparison of shear stress distribution.

Tunneling profiles were obtained by digitizing crack fronts in post-fatigued SENB specimens (Figure 2) that had been monotonically loaded to discrete levels of crack extension. To accommodate the numerical model and provide several tunneling profiles to be prescribed as crack extension steps, these discrete tunneling patterns were curve fit and interpolated at intermediate locations. The result of this process is shown in Figure 8 where Tx-3PB are experimentally obtained levels of crack extension. Figure 9 shows the application of the curved crack front shape as constrained nodes in the finite element model. As the crack extends, these constrained nodes are released in such a manner as to follow the natural tunneling profiles shown in Figure 8.

4 Post Processing and Calculation of T_{ϵ}^*

Following closely the work of Nikishkov and Atluri (1987), a formulation for numerical calculation of the T_{ϵ}^* integral using stress, strain, and displacement data output from ABAQUS may be obtained. Beginning with a vector representation and employing the EDI formulation, the T_{ϵ}^* integral may be represented as

$$T_{1\epsilon}^* f = - \int_{A-A_{\epsilon}} \left(W n_1 - \sigma_{ij} \frac{\partial u_i}{\partial x_1} n_j \right) s dA \quad (2)$$

where $s(x_1, x_2, x_3)$ is an arbitrary function equal to 1 on Γ_{ϵ} , and 0 on a far field contour, Γ , and f is the area under this s -function along a particular segment of the crack front (Figure 10). Then, by application of the divergence theorem,

$$\begin{aligned} T_{1\epsilon}^* f = & - \iiint_{V-V_{\epsilon}} \left(W \frac{\partial s}{\partial x_1} - \sigma_{ij} \frac{\partial u_i}{\partial x_1} \frac{\partial s}{\partial x_j} \right) dV \\ & - \iiint_{V-V_{\epsilon}} \left(\frac{\partial W}{\partial x_1} - \frac{\partial}{\partial x_j} \left(\sigma_{ij} \frac{\partial u_i}{\partial x_j} \right) \right) s dV \\ & + \int_{A_1+A_2} \left(W n_k - \sigma_{ij} \frac{\partial u_i}{\partial x_1} n_j \right) s dA \end{aligned} \quad (3)$$

where $V - V_{\epsilon}$ is the volume enclosed within the EDI region, and $A - A_{\epsilon}$ is the area of the ends of the annular volume.

In order to facilitate numerical integration, parametric representations of displacements, coordinates, and s -functions are utilized as in Eq. 4 where N^I are quadratic shape functions, $N^I = N^I(\xi, \eta, \zeta)$ and I is a node number.

$$\begin{aligned} s &= N^I s^I \\ x_i &= N^I x_i^I \\ u_i &= N^I u_i^I \end{aligned} \quad (4)$$

Following substitution of Eqs. 4 into Eq. 3, the integral was solved numerically via 2x2x2 Gaussian quadrature. Since the FE solver outputs integration point, or nodal values of relevant quantities, the implementation of this numerical integration is relatively straightforward in Matlab, or Fortran. Full details of the formulation development may be found in Nikishkov and Atluri (1987) where the formulation for incremental J -integral is developed.

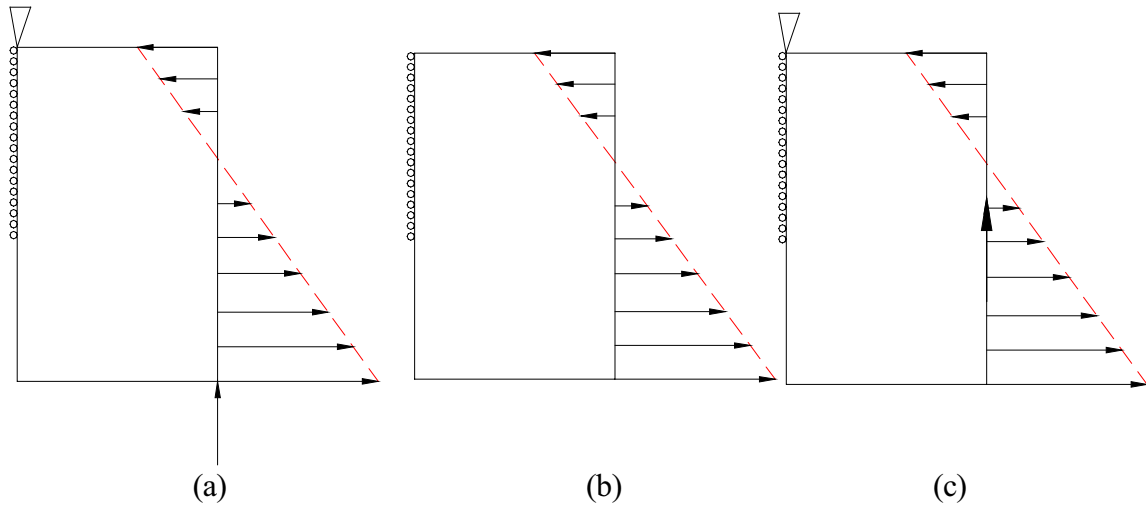


Figure 6 : Transverse displacement boundary conditions applied at truncation boundary.

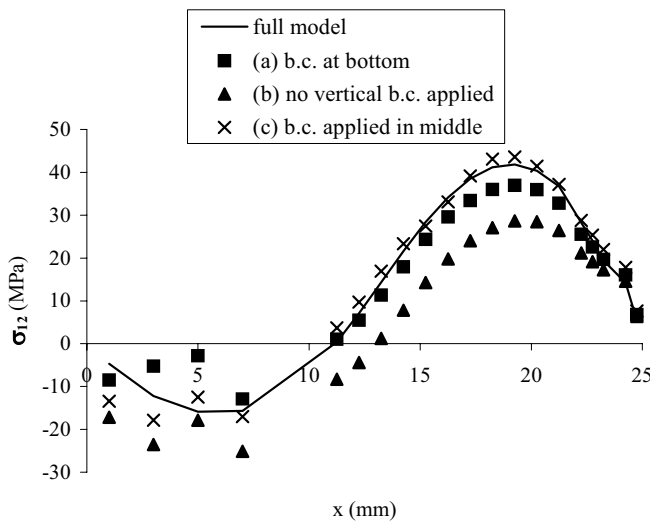


Figure 7 : Shear stress distribution through specimen width near boundary for $\Delta a = 0.00$ mm.

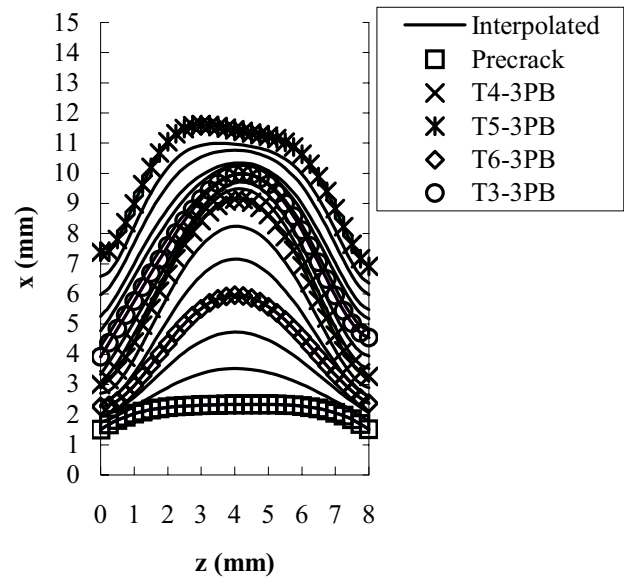


Figure 8 : Interpolated crack front profiles.

4.1 Integration Contour Details

To avoid numerical difficulties and to ensure a valid comparison between T_{ϵ}^* values obtained at the surface of the specimen, and the through-thickness values, a similar size contour must be used. This contour should be such that an assumption of near 2-D behavior can be made if this comparison is to be drawn. An examination of the out-of-plane strains (ϵ_{33}) directly in front of the crack tip shows that after a short amount of crack extension, the

level of out-of-plane strain becomes constant at a specific distance ahead of the crack tip. Figures 11 and 12 show the extent of out-of-plane strain (with respect to the $x - y$ plane) through the thickness of the numerical model at different distances, r , from the crack tip for crack extensions of $\Delta a = 0.0$ mm, and $\Delta a = 0.75$ mm, respectively. This attainment of a constant value of ϵ_{33} is indicative of a transition to a plane strain state at a distance from the crack tip corresponding to this value of r . Since there is

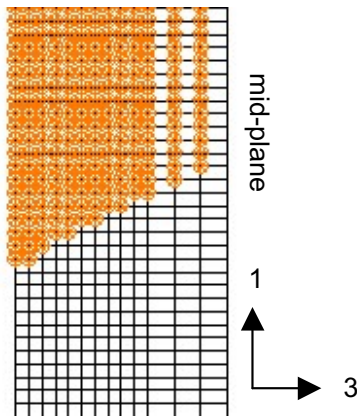


Figure 9 : Application of tunneling profile at crack tip.

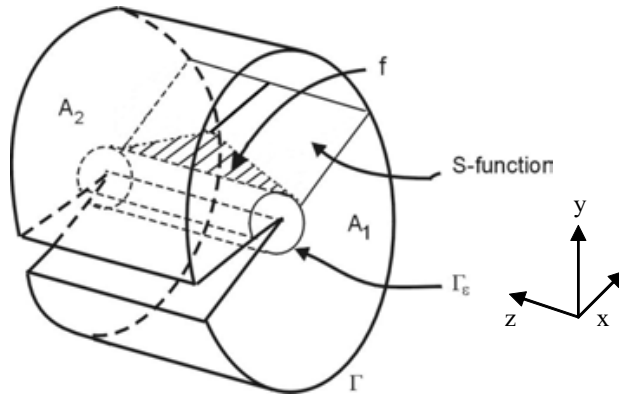


Figure 10 : EDI Formulation.

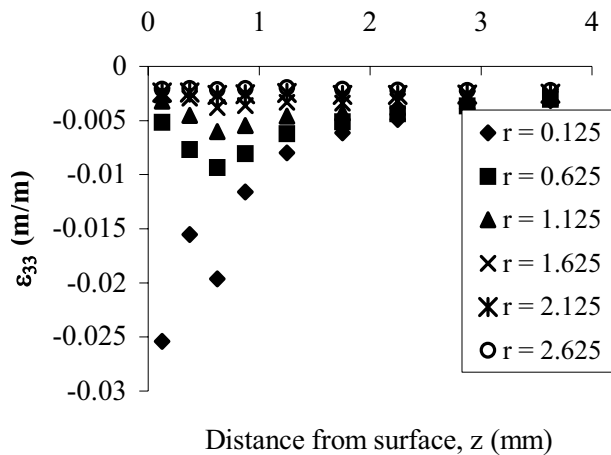


Figure 11 : Out of plane strain, ϵ_{33} for $\Delta a = 0.00$ mm.

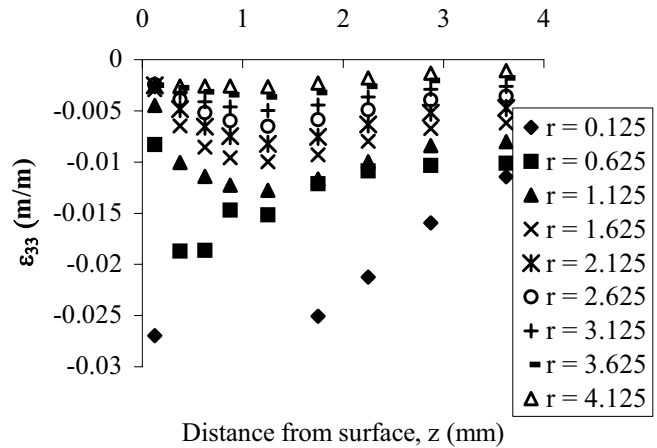


Figure 12 : Out of plane strain, ϵ_{33} for $\Delta a = 0.75$ mm.

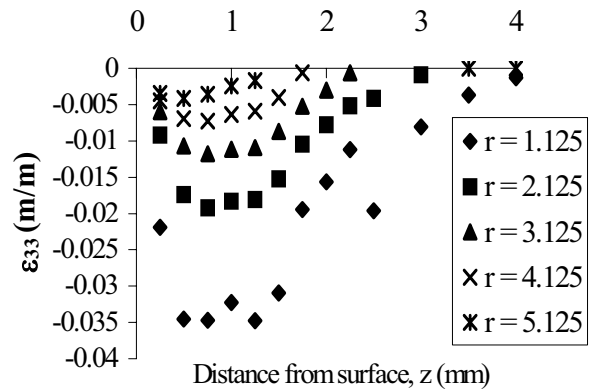


Figure 13 : Out of plane strain, ϵ_{33} for $\Delta a = 3.00$ mm.

now a level of constancy through the thickness, this distance can be used as the inner, Γ_ϵ contour size, ϵ . For a short amount of crack extension (0.75 mm), it is seen that this transition begins to occur at a distance of approximately 1 mm and that out of plane strain becomes essentially constant and very close to zero between 2 and 3 mm from the crack tip. Figure 13 shows strain behavior after several crack extension steps. Here, it is seen that the distance for plane strain transition increases to between 3 and 4 mm from the crack tip. A paper by Narisimhan and Rosakis (1990) discussed a correlation between specimen thickness and distance to this plane state transition for plane stress specimens. It was found that the distance to the transition point was roughly equivalent to half the specimen thickness in correlation with what is seen here in Figures 11, 12 and 13 for the near surface, plane stress portions.

The extent of tunneling seen in this analysis leads to numerical difficulties with regard to explicitly prescribing the aforementioned transition point as the exact location of the inner, Γ_ϵ integration contour. A preliminary inspection of the behavior of the T_ϵ^* integral through the thickness of the specimen after a few crack extensions revealed sensitivity of the analysis to the location of the integration contour. After a short amount of crack propagation, the expected path dependency of the T_ϵ^* integral becomes very evident. For contour sizes of 1.0, 2.0 mm, and 3.0 mm, the behavior of the local crack tip integral can change by 10-20%. There is also a slight dependence of T_ϵ^* integral on the size of the EDI region. Since the T_ϵ^* calculation should be independent of EDI domain size [Nishioka, Kobayashi, and Epstein (1993)], this dependence is indicative of numerical errors due to loss of stress and strain data as the crack tip is approached and extreme plasticity is present or, possibly boundary effects if a large enough contour is used. It is also indicative of a loss of resolution since the s -function is assigned at node points, based on their location within the EDI boundaries. Fewer node points through the width of the EDI region will obviously adversely affect the accuracy of the calculation. As an example, if the extreme cases of either only one element through the EDI region width or, say four elements through the EDI region width are considered, it is easy to see that the former case will utilize s -function values of 1 and 0, whereas the latter would have s -functions of 1, 0.75, 0.5, 0.25, and 0 as the EDI region is traversed. Thus, very small, or very large contour sizes should be avoided due to the numerical inaccuracies and a reasonable number of elements through the EDI region should be assigned.

Inspection of Figures 11 and 12 reveal that an integration contour size of less than 1.0 mm would likely lead to erroneous results. For distances, $r=0.125$ and $r=0.625$, the out-of-plane strain changes dramatically, depending on through-thickness location. However, since the T_ϵ^* integral is supposed to be a “near tip” parameter, the contour size should be kept as small as possible. Figures 11 and 12 reveal that at a distance of $r=1.125$ mm, the variation of out-of-plane strain was much lower and that at larger values of r , the variation does not significantly improve. Figure 13 shows this trend starting at between $r=2.125$ mm and $r = 3.125$ mm. Based on the out of plane strain plots, a contour size of $\epsilon = 2.0$ mm makes the most sense in terms of maintaining a close proximity to the crack

tip and, at the same time, allowing a valid comparison to experimental T_ϵ^* values obtained on the surface.

4.2 Crack Front Coordinate Transformation

To accommodate the tunneling crack front, which is continually turning with respect to the thickness, the global variables are normally transformed with respect to the crack front coordinate system to “straighten” the crack front. This becomes more and more of an issue as the inner contour of integration is collapsed onto the crack tip. The coordinate transformation simply involves calculating local tangents to the crack front and transforming stresses, strains, work densities, displacements, and coordinates to the crack front coordinate system. These transformations from global to local coordinates are applied in the x - z plane (plane of the crack) and are simply:

$$\begin{aligned} x_i &= a_{ij}x_j^G \\ s_{ij} &= a_{ip}a_{jq}s_{pq}^G \end{aligned} \quad (5)$$

for vectors, and tensors respectively. However, as the inner contour of integration is moved further away from the crack tip, the transformation of global variables to the crack front coordinate system becomes less reasonable. Instead, a rotation of the entire EDI region with respect to the global coordinate system is likely required in addition to the transformation of global variables. This is an extremely complex operation that would require a very refined, radial mesh surrounding the current crack tip. The mesh would also need to adapt intelligently as the crack tip moves. Figure 14 is a representation of the effect of transforming the variables within the EDI region and of transforming the EDI variables in addition to a rotation of the entire EDI region with respect to the crack front. Since this is not feasible for the current numerical model, T_ϵ^* is estimated without any transformation of the EDI quantities. Thus, the result should be interpreted as more of a “global” value of the energy release rate. Regardless of contour size, the integration is performed over elements sufficiently far from the crack front to allow this approximation, especially after several steps of crack extension where the contour has extended far behind the current crack tip. Additionally, it is noted that in the present numerical analysis, element layers are locally straight with respect to the global model coordinate system (Figure 9).

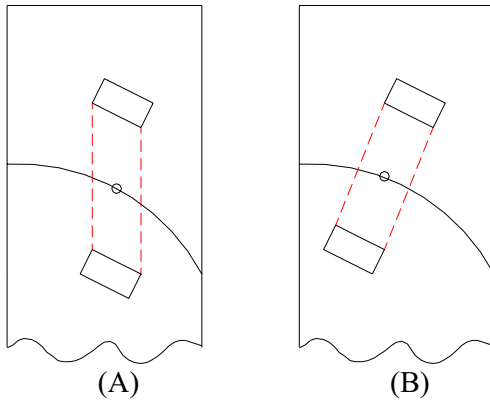


Figure 14 : Transformation of EDI variables (A) and transformation of EDI variables with rotation (B).

4.3 *S*-function

The *s*-function is an arbitrary, smooth function that varies from a value of 1.0 on the inner, Γ_ϵ contour, to 0.0 on the outer contour. Several possibilities for this function are discussed in Nikishkov and Atluri (1987), including a linear *s*-function and triangular *s*-function, which are the two chosen as candidates for this work. The linear *s*-function is slightly simpler, geometrically and allows a domain calculation at each element interface, but requires that the ends of the annular domain be included in the calculation. On the other hand, the triangular *s*-function, which was used for the final analysis requires two element layers per calculation but removes the ends of the domain volume from the analysis. Performing two calculation passes, each offset by one element as illustrated in Figure 15 solves the resolution problem.

5 Numerical Results

5.1 T_ϵ^* integral

T_ϵ^* was calculated for each of seventeen, 0.25mm and 0.50 mm crack extension steps, with the extent of experimentally observed tunneling reflected in the crack face boundary conditions at each step. Using a post-processing program written in Matlab that utilizes output from ABAQUS, point-wise values were obtained at each layer interface through the thickness of the quarter model to build a plot of behavior for the extending, tunneling crack. Since the integration program utilized the triangu-

lar *s*-function, values were unobtainable on the extreme surface, and center plane. The remaining values provide adequate resolution, so this is not a major problem.

Figure 16 shows the variation of T_ϵ^* through the thickness of the specimen at four different locations along the crack front. It is noted that T_ϵ^* remains fairly constant near the highly constrained mid-plane ($z = 4.0$ mm), but exhibits a rising trend as the plane stress surface is approached.

Figures 17-19 show T_ϵ^* calculated on contours of 3.0, 2.0, and 1.0 mm, respectively. Pointwise values are reported at each element interface through the thickness (z) direction. Problems with excessive noise caused by extreme deformation are evident in Figure 19 for T_ϵ^* calculated on an integration contour of 1.0 mm.

5.2 *CTOA* variation

The Crack Tip Opening Angle (*CTOA*) was also calculated using the displacements normal to, and behind the crack front as the crack extended.

Figure 20 shows the *CTOA* calculated at three locations through the thickness at approximately 1.0 mm behind and normal to the crack tip for the surface, the quarter point (midpoint of numerical model), and the specimen mid-point. The surface *CTOA* trend shows the typical sharp increase at the beginning of crack growth, followed by a decline to a fairly steady state value of approximately 7-8 degrees. The quarter point and mid-point trends exhibit an interesting slow rise as the crack extends. This behavior is due to the rapid crack propagation in the center (tunneling) near the beginning of the test, which will produce a small amount of crack tip blunting and hence low *CTOA*. As the tunneling slows, the *CTOA* on the inner layers should increase as seen here due to increasing amounts of plastic deformation and crack tip blunting. It is observed that the *CTOA* roughly follows the same trend as the near-field T_ϵ^* calculated on an $\epsilon = 1.0$ mm contour. Both the *CTOA* and the near-field T_ϵ^* show a decreasing trend followed by a fairly sharp increase at local crack extensions longer than approximately 6.0 mm.

6 Discussion

The numerically obtained T_ϵ^* shows a decreasing trend as the mid-plane is approached which is contrary to energy release rate behavior up to the point of crack initiation seen in previous studies involving *J*-integral. However,

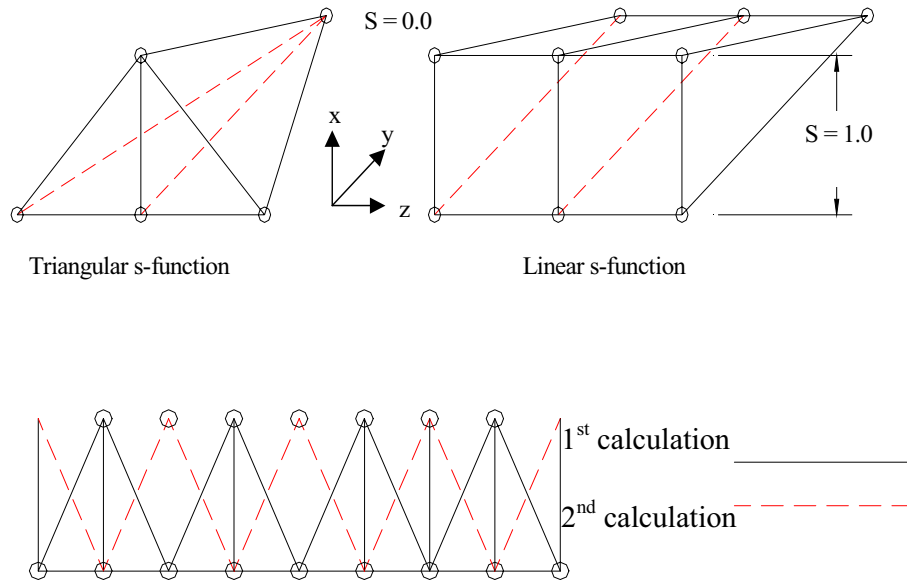


Figure 15 : Triangular and Linear s-functions with scheme to increase calculation resolution.

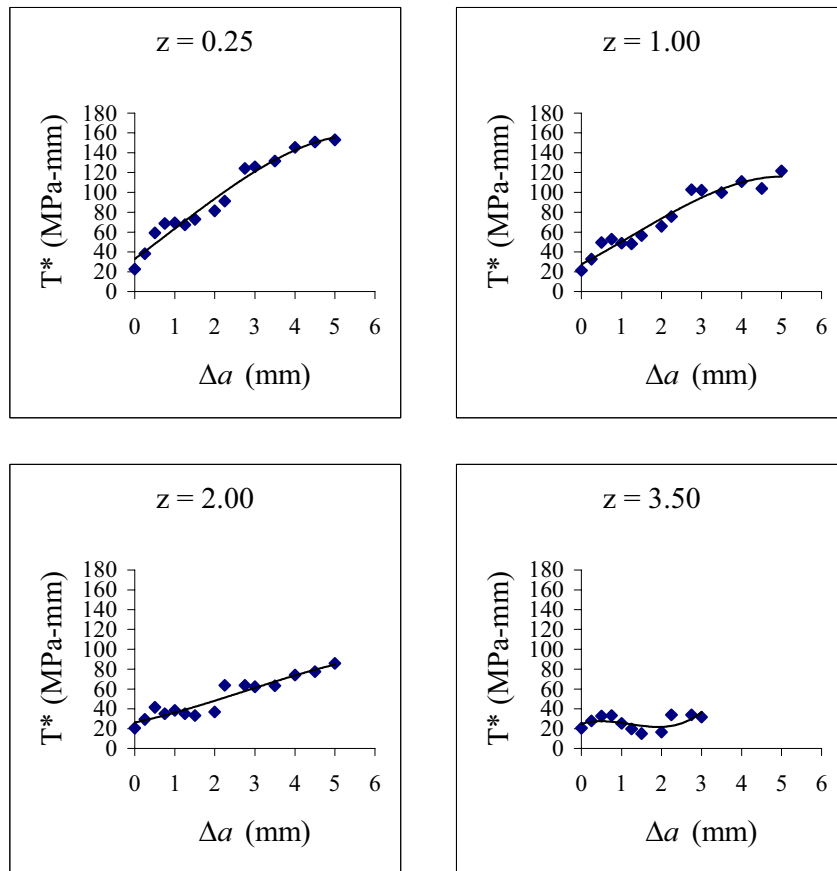


Figure 16 : T^*_ϵ for extending crack at various through-thickness locations $\epsilon = 3.0$ mm.

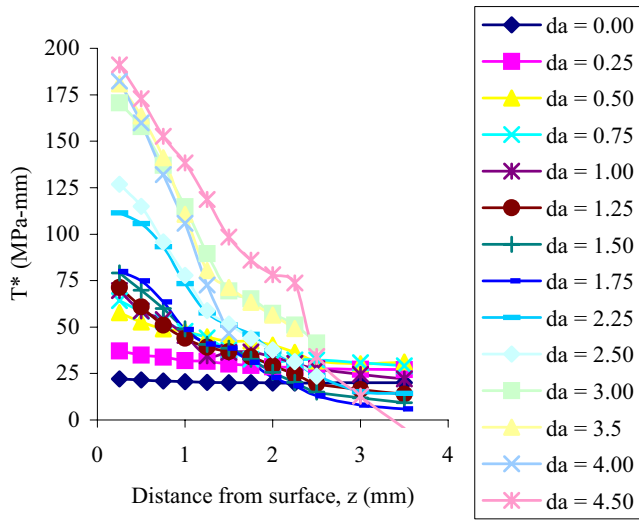


Figure 17 : T_{ϵ}^* for an integration contour, $\epsilon = 3.0$ mm.

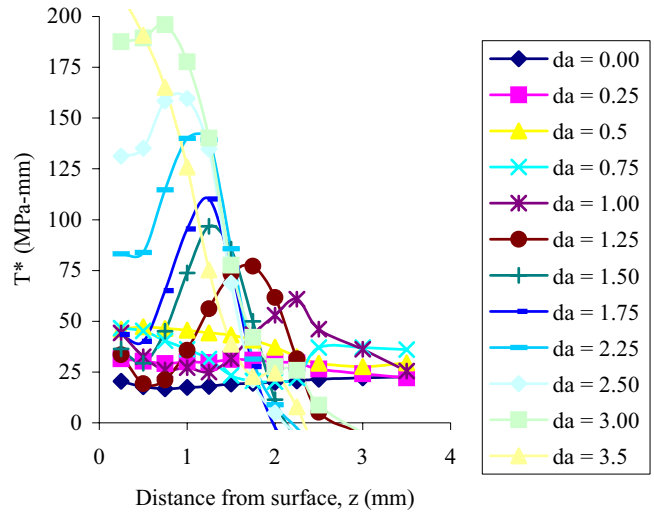


Figure 19 : T_{ϵ}^* for an integration contour, $\epsilon = 1.0$ mm.

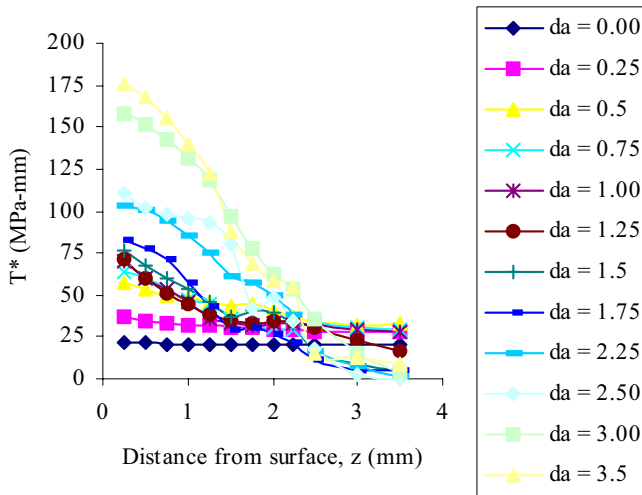


Figure 18 : T_{ϵ}^* for an integration contour, $\epsilon = 2.0$ mm.

the extreme tunneling should not directly imply a trend of rising crack driving force toward the center. It is instead a result of lower resistance near the mid-plane, which is reflected in the lower T_{ϵ}^* values at this crack front location. The specimen being modeled is relatively thick and will exhibit a fairly thin region of plane stress near the surface and transition to a plane strain state as the mid-plane is approached. This trend is seen directly in the plots of ϵ_{33} shown in Section 4.1 (Figures 11-13). In light of this, T_{ϵ}^* should instead be compared to a more local, physical parameter such as $CTOA$. This comparison is best made

with the T_{ϵ}^* calculated on an $\epsilon = 1.0$ mm contour size since $CTOA$ is local to the crack tip. As the mid-plane of the specimen is approached and for extensive tunneling, the T_{ϵ}^* extending contour integral begins to exhibit characteristics similar to those of a T_{ϵ}^* integral calculated with a moving contour as seen by Okada, Omori, Atluri, and Kobayashi (1999). It is likely that the reason for this is the decreasing contribution from those portions of the contour in the wake of the extending crack. That is, each step in this case is more similar to a case of T_{ϵ}^* calculated on a truncated contour as the strain history never builds as in the case of a controlled, stably growing crack. Regardless, some comparison must be drawn between mid-plane and surface T_{ϵ}^* in order to allow the use of experimentally obtained values to predict crack extension throughout the thickness of a specimen.

At crack initiation, and within the first few steps of crack growth, the surface and mid-plane values are quantitatively similar. However, as the crack extends, the surface T_{ϵ}^* rapidly increases while the mid-plane value stays fairly steady, with a slight trend toward rising. After approximately 5-6 mm of crack growth, the two reach a steady state with respect to each other and a comparison can be made between the plane stress (surface) values and plane strain (mid-plane) values.

For the linear elastic case, a comparison of J_C and J_{IC} for very thin specimens (plane stress) and thick specimens (near plane strain) respectively is made for 2024-

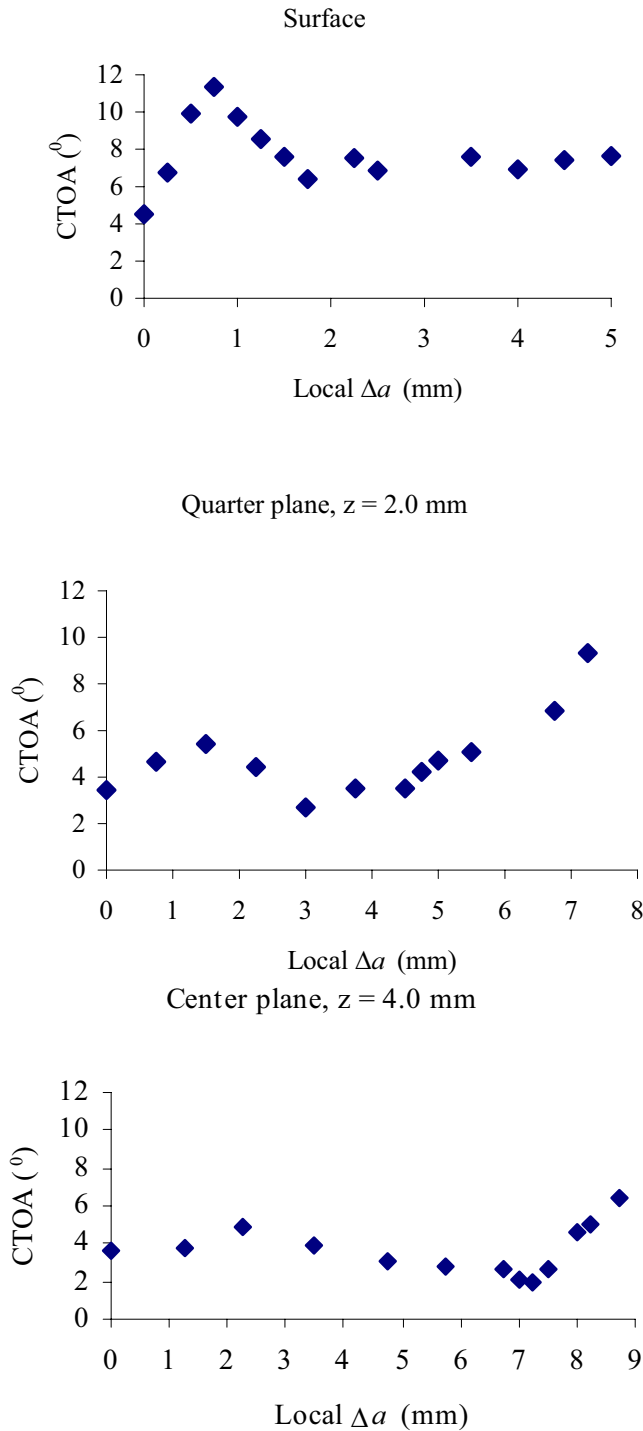


Figure 20 : CTOA variation through the specimen thickness.

T3 aluminum alloy as (K values from Batelle, Columbus (1975));

$$\left(\frac{K_{IC}}{K_C^{t=0.8mm}}\right)^2 \frac{1}{(1-\nu^2)} = \left(\frac{33 \text{ MPa}\sqrt{m}}{115 \text{ MPa}\sqrt{m}}\right)^2 \frac{1}{(1-.34^2)} = 0.09 \quad (6)$$

which shows plane strain J_{IC} to be roughly 9% of plane stress J_C . Since J -integral is incapable of characterizing the crack tip behavior after crack extension, this comparison cannot realistically be made for the case of long crack extension and extreme tunneling. However, this comparison can be used to make an analogy to the behavior of a steady state T_ϵ^* toughness behavior since this would represent the “critical” value of T_ϵ^* . An inspection of the plots of T_ϵ^* for all contour sizes, and especially the very near-tip $\epsilon = 1.0$ mm contour reveals a relationship between plane stress (surface) T_ϵ^* and plane strain (mid-plane) T_ϵ^* . While the 3-point bend specimen configuration did not allow sufficient crack extension to achieve the complete steady state T_ϵ^* value, it comes close enough to begin to show signs of achieving a steady state value which should occur at a crack extension roughly equivalent to half the specimen thickness. At the final point of crack extension (5.0 mm on the surface), the ratio between surface T_ϵ^* and mid-plane T_ϵ^* is roughly 10 %, regardless of contour size, or method of calculation. The much lower plane strain T_ϵ^* is a direct reflection of the much lower resistance to crack extension in the plane strain region in comparison to the surface, plane stress region. The very close agreement with the ratio of linear elastic fracture toughnesses is encouraging since this would indicate the possibility for using plane stress (surface) T_ϵ^* values to predict the fracture resistance on the interior of a thick specimen.

In a study by Ma, Kobayashi, Atluri and Tan (2000), plane stress T_ϵ^* was calculated for thin, 0.8 mm thick 2024-T3 aluminum center notched specimens to be approximately 170 Mpa-mm at steady state. This compares favorably with the results of this study for calculation of T_ϵ^* at the specimen surface. The surface value in the current study was approximately 175 Mpa-mm. The correlation between the current results and those previously published is promising.

It is noted that in the time between completion of this work and its final publication, substantial progress has

been made in the area of numerical analysis of fracture mechanics problems using the Meshless Local Petrov Galerkin (MLPG) method outlined in the book by Atluri and Shen (2003). The reader is additionally referred to a number of recently published papers for details regarding utilization of the MLPG method, including: Han and Atluri (2003); Li, Shen, Han, and Atluri (2003); Atluri, Han, Shen (2003); Han and Atluri (2002); Atluri and Shen (2002).

7 Conclusions

T_{ε}^* values generally reach a peak of approximately 175 MPa-mm on the surface and approximately 30 MPa-mm in the mid-plane. This significant difference is due to the existence of a plane stress state at the extreme surface, and a plane strain region at the mid-plane of the specimen.

T_{ε}^* for the 3-D configuration and tunneling crack front behaves similarly to the local crack tip parameter, $CTOA$ for corresponding through-thickness resistance curves. Thus, local T_{ε}^* is assumed to represent the point-wise energy inflow to the crack front.

T_{ε}^* is very sensitive to the constraint level in the material surrounding the crack tip and will exhibit distinct plane stress and plane strain values. The ratio of the plane strain T_{ε}^* and plane stress T_{ε}^* values is approximately 10% for this material and specimen geometry.

Acknowledgement: This work was sponsored by a U.S. Department Of Energy Grant 03-97ER14770.

References

Amestoy, M.; Bui, H. D.; Labbens, R. (1981): On the definition of local path independent integrals in three-dimensional crack problems. *Mechanics Research Communications*, vol. 8, no. 4, pp. 231-236.

Atluri, S. N.; Nishioka, T.; Nakagaki, M. (1984): Incremental path-independent integrals in inelastic and dynamic fracture mechanics. *Engineering Fracture Mechanics*, vol. 20, no. 2, pp. 209-244.

Atluri, S. N.; Shen, S. (2002): The Meshless Local Petrov-Galerkin (MLPG) Method: A Simple, Less-costly Alternative to the Finite Element and Boundary Element Methods, *CMES: Computer Modeling in Engineering & Sciences*, Vol. 3, No. 1, pp. 11-52.

Atluri, S. N.; Shen, S. (2003): *The Meshless Local Petrov-Galerkin (MLPG) Method*, CREST Monograph Series No. 1, Tech Science Press.

Atluri, S. N.; Han, Z. D.; Shen, S. (2003): Meshless Local Petrov-Galerkin (MLPG) Approaches for Solving the Weakly-Singular Traction Displacement Boundary Integral Equations, *CMES: Computer Modeling in Engineering & Sciences*, Vol. 4, No. 5, pp. 507-518.

Battelle Columbus Laboratories. (1975): *Damage Tolerant Design Handbook*, Metals And Ceramics Information Center, Battelle Columbus Laboratories, Columbus, OH.

Brust, F. W.; McGowan, J. J.; Atluri, S. N. (1986): A combined numerical/experimental study of ductile crack growth under a large unloading using T^* , J , and $CTOA$ criteria. *Engineering Fracture Mechanics*, vol. 23, no. 3, pp. 537-550.

Brust, F. W.; Nishioka, T.; Atluri, S. N., Nakagaki, M. (1985): Further studies on elastic-plastic stable fracture utilizing the T^* integral. *Engineering Fracture Mechanics*, vol. 22, no. 6, pp. 1079-1103.

Han, Z. D.; Atluri, S. N. (2002): SGBEM (for Cracked Local Subdomain) – FEM (for uncracked global Structure) Alternating Method for Analyzing 3D Surface Cracks and Their Fatigue-Growth. *CMES: Computer Modeling in Engineering & Sciences*, Vol. 3, No. 6, pp. 699-716

Han, Z. D.; Atluri, S. N. (2003): Truly Meshless Local Petrov-Galerkin (MLPG) Solutions of Traction Displacement BIEs. *CMES: Computer Modeling in Engineering & Sciences*, Vol. 4, No. 6, pp. 665-678.

Li, F. Z.; Shih, C. F.; Needleman, A. (1985): A comparison of methods for calculating energy release rates. *Engineering Fracture Mechanics*, vol. 21, no. 2, pp. 405-421.

Li, Q.; Shen, S.; Han, Z. D.; Atluri, S. N. (2003): Application of Meshless Local Petrov-Galerkin (MLPG) to Problems with Singularities, and Material Discontinuities, in 3-D Elasticity. *CMES: Computer Modeling in Engineering & Sciences*, Vol. 4, No. 5, pp. 571-586

Ma, L.; Kobayashi, A. S.; Atluri, S. N.; Tan, P. W. (2000): Crack linkup by stable crack growth. *CMES: Computer Modeling in Engineering & Sciences*, vol. 1, no. 4, pp. 19-26.

Nakamura, T.; Shih, C. F.; Freund, L. B. (1986):

Analysis of a dynamically loaded three-point bend ductile fracture specimen. *Engineering Fracture Mechanics*, vol. 25, no. 3, pp. 323-339. no. 5, pp. 625-643.

Narasimham, R.; Rosakis, A. J. (1990): Three-Dimensional Effects Near a Crack Tip in a Ductile Three-Point Bend Specimen: Part I-A Numerical Investigation. *Journal of Applied Mechanics*, Vol. 57, pp. 607-617.

Nikishkov, G. P.; Atluri, S. N. (1987): Calculation of fracture mechanics parameters for an arbitrary three-dimensional crack, by the 'Equivalent Domain Integral' method. *International Journal for Numerical Methods in Engineering*, vol. 24, no. 9, pp. 1801-1821.

Nishioka, T.; Kobayashi, Y.; Epstein, J. S. (1993): On the near-tip deformation in inhomogeneous elastic-plastic fracture specimens: part 2 – finite element simulation. *Pressure Vessel Integrity – 1993: Proceedings of the 1993 Pressure Vessels and Piping Conference, Denver CO*. PVP-Vol. 250, ASME.

Okada, H.; Atluri, S. N.; Omori, Y.; Kobayashi, A. S. (1999): Direct evaluation of T_{ϵ}^* integral from experimentally measured near tip displacement field, for a plate with stably propagating crack. *International Journal of Plasticity*, vol. 15, no. 9, pp. 869-897.

Parks, D. M. (1977): The virtual crack extension method for nonlinear material behavior. *Computer Methods in Applied Mechanics and Engineering*, vol. 12, pp. 353-364.

Li, Q.; Shen, S.; Han, Z. D.; Atluri, S. N. (2003): Application of Meshless Local Petrov-Galerkin (MLPG) to Problems with Singularities, and Material Discontinuities, in 3-D Elasticity. *CMES: Computer Modeling in Engineering & Sciences*, Vol. 4, No. 5, pp. 571-586

Raymund, M.; Palusamy, S. S. (1981): J -integral for 3-D with center-cracked plate tests. *Computers and Structures*, vol. 13, pp. 691-697.

Rice, J. R. (1968): A path independent integral and the approximate analysis of strain by notches and cracks. *Journal of Applied Mechanics*, vol. 35, pp. 379-386.

Shih, C. F.; Moran, B.; Nakamura, T. (1986): Energy release rate along a three-dimensional crack front in a thermally stressed body. *International Journal of Fracture*, vol. 30, no. 2, pp. 79-102.

Stonesifer, R. B.; Atluri, S. N. (1982): On a study of the (ΔT) and C^* integrals for fracture analysis under non-steady creep. *Engineering Fracture Mechanics*, vol. 16,

